Paper presented at the International Conference
on the Spectroscopy of Heavy Nuclei, Crete, Greece, 25 June - 1 July, 1989.

CONF-890686--2

Alpha-Particle and Proton Probes of Nuclear Shapes in the Rare Earth and Mass 80 Regions

D.G. Sarantites, N.G. Nicolis, V. Abenante, Z. Majka, T.M. Semkow
Washington University, St. Louis, MO 63130
and
C. Baktash, J.R. Beene, G. Garcia-Bermudez, M.L. Halbert, D.C. Hensley,
N.R. Johnson, I.Y. Lee, F.K. McGowan, M.A. Riley, A. Virtanen
Oak Ridge National Laboratory, Oak Ridge, TN 37830
and
H.C. Griffin
University of Michigan, Ann Arbor, MI 48109

CONF-890686--2
DE90 000725

ABSTRACT: Low emission barriers and large subbarrier anisotropies in the alpha-particle decay with respect to the spin direction, of Sn and rare earth compound nuclei, are examined in the light of recent calculations incorporating deformation. To explore the possibility of a correlation between the proton emission barriers and nuclear deformation, we studied proton spectra from the $^{52}Cr(^{34}S,2p2n)^{82}Sr$ reaction. The proton spectra were observed with the Dwarf-Ball 4π CsI(Tl) array, in coincidence with 18 Compton suppressed Ge detectors operated in conjunction with the Spin Spectrometer, a 4π NaI(Tl) array. We found significant changes and shifts in the proton energy spectra as we selected gating transitions from bands of different moments of inertia or transitions from states of different spin in the same band. Substantial differences were also seen as a function of the γ-ray multiplicity. These results are discussed in terms of statistical model calculations incorporating deformation and structure effects of the emitting system.

1. INTRODUCTION.

The study of nuclear shapes at high angular momentum and excitation energy is a topic of current extensive theoretical and experimental interest in heavy-ion physics. It is well known that collective nuclei near the yrast line are deformed and their structure is well described by liquid-drop-Strutinsky cranked shell model calculations. A question of interest is the evolution of these shapes as the spin and the excitation energy (temperature) are increased. There is already considerable experimental evidence for the existence of superdeformed nuclei ($\beta = 0.6$) at high spins.[1] Theoretical calculations

that explain these highly deformed shapes predict even higher deformations ($\beta \approx 0.9$) for nuclei close to the fission stability limit[2,3]. Temperature-induced noncollective rotation in nuclei, as well as shape changes have also been discussed in connection with predictions of mean field theories.[4] A number of experimental studies have tried to explore the effect of high excitation and/or angular momentum degrees of freedom on the nuclear shapes. This is made, on one hand, by exploiting the γ-decay properties (for example, study of giant resonances built on excited states) of the deexciting compound nuclei[5]. On the other hand, extensive searches are being made to find signatures of shape effects in the charged-particle decay properties of such systems[6–12].

The motivation for light charged particle studies lies in the well established fact that (fission-stable) compound nuclei, with the highest possible angular momentum, often decay by emitting alpha particles and protons. If the deexciting nucleus is deformed, it exhibits a lower evaporation barrier along the longer axis for charged-particle emission, compared to the spherical case. This results in strong enhancements of α and proton decay along the long axis, especially in the energy region below the evaporation Coulomb barrier[6,7,12]. Simulation studies along these lines have motivated a number of experiments consisting of the observation of α-particle spectra in heavy-ion fusion-evaporation reactions in a singles mode or in coincidence with evaporation residues[7,11,12]. The inability to reproduce the subbarrier part of the observed α-spectra, with statistical model calculations assuming spherical emission shapes, has been used as an indication of a deformation effect.

The desire for an unconstrained experimental study of these effects led us to the development of the spin alignment method with the Spin Spectrometer[13], a highly segmented 4π γ-ray detector system. In this method, the magnitude and orientation of the spin of the residual nuclei is deduced on an event-by-event basis. This makes possible detailed studies, such as the measurement of α-particle angular distributions with respect to the spin direction[14]. Furthermore, the γ-multiplicity selection with the spin spectrometer allows us to study these decay characteristics as a function of the evaporation residue spin, which is closely correlated to the compound nucleus spin. Therefore, the alpha-decay properties of different compound nuclear systems can be studied in detail[8–10].

In the first part of this paper, we report on the results of an earlier survey study[10] concering α-particle energy spectra and angular distributions with respect to the spin direction for a number of compound nuclear systems. The two typical cases of the closed shell ^{114}Sn* and the rare earth ^{170}Yb* deexciting compound nuclei are compared. The alpha emission properties of these systems are described by the anisotropy coefficients of the alpha particle emission with respect to the spin direction as a function of the α-particle energy and γ-ray multiplicity. Differences in the emission patterns,

in the energy region below the evaporation Coulomb barrier, suggest nearly spherical and deformed emission shapes in the cases of $^{114}Sn^*$ and $^{170}Yb^*$, respectively.

Detailed statistical model calculations have been performed to clarify the deviations of the "deformed" versus the "spherical" behaviour. In the subbarrier region, the predictions of the statistical model for charged particle emission are sensitive to barrier penetration effects. These effects are expressed in terms of transmission coefficients resulting from an optical model calculation. Although our statistical model calculations describe closely the decay of $^{114}Sn^*$, we observe discrepancies in the other system. These descrepancies, appear as (a) an underestimate of the subbarrier 90° CM spectra, (b) underestimates of the multiplicity-gated 90° CM spectra, which increase with spin, and (c) deviations in the trend of the anisortopy coefficients from the one predicted in the $^{114}Sn^*$ case, which also increase with spin. We show that a simulation of deformation effects due to transmission accounts for these discrepancies. A detailed comparison with the $^{170}Yb^*$ data is made, which shows the angular momentum dependence of the deformation effect in the α spectra. However, more elaborate calculations are required to describe the corresponding effect in the anisotropy coefficients of these systems. The above findings are corroborated by both the known ground state properties and data of giant resonances built on excited states of similar compound nuclear systems.

In the second part of this paper, we report on experimental results of an attempt to explore the possibility of a correlation between the proton emission barriers and nuclear deformation and/or structure. Proton spectra from the $^{52}Cr(^{34}S,2p2n)^{82}Sr$ reaction at 130 MeV have been studied in coincidence with discrete γ transitions of selected exit channels. The proton spectra were observed with the Dwarf-Ball array[15], a 72 Cs(Tl) 4π detector, in coincidence with 18 Compton suppressed Ge detectors. This system operated in conjunction with the Spin Spectrometer which recorded the associated γ-ray multiplicity. We found significant changes and shifts in the proton energy spectra as we selected gating transitions from bands of different moments of inertia or transitions from states of different spin in the same band. Substantial differences were also seen as a function of the γ-ray multiplicity. The above results will be discussed in terms of statistical model calculations incorporating deformation and structure effects of the emitting system.

2. ALPHA EMISSION PROPERTIES AND DEFORMATION EFFECTS.

The experiments in this work were performed at the Oak Ridge Holifield Heavy-Ion Research Facility (HHIRF). The compound systems studied were: $^{110}Sn^*(E^* = 93.9$ MeV), $^{114}Sn^*(79.5$ MeV), $^{138}Nd^*$, $^{164}Yb^*$ (67.2 MeV) and $^{170}Yb^*(134.8$ MeV). The details of the experimental method and some of the general features of the data

can be found in the current literature.[8,9,10,14] The complete study is in the process of publication. In the discussion below, we limit ourselfs to the presentation of distinct features shown in the deexcitation data of ^{114}Sn* and ^{170}Yb*.

The compound nuclei ^{114}Sn* and ^{170}Yb* were produced in the reactions ^{64}Ni(250 MeV) + ^{50}Ti $\rightarrow$ ^{114}Sn* and ^{20}Ne(176.6 MeV) + ^{150}Nd $\rightarrow$ ^{170}Yb*, respectively. In this study, self-supporting targets of high isotopic enrichment in each of the isotopes were used. The α-particles emitted in the deexcitation of the above compound nuclei were recorded by Si surface barrier telescopes positioned at the laboratory angles corresponding to $\sim 90°$ in the center-of-mass system.

The ΔE detectors had thickness of 65 μm and an acceptance cone of $\sim 6°$ half angle. The E detectors were 1500 μm thick and served as the triggers of the spin spectrometer. The spin spectrometer served as the γ-ray detector and measured simultaneously the γ-ray multiplicity, M_γ, the total γ-ray deexcitation energy and the γ-ray angular correlations. In these experiments the spin spectrometer provided a coverage of 95.8% of 4π sr.

For each compound nuclear system (A_{CN}, Z_{CN}), the alpha-particle events were transformed in the center-of-mass system for α + (A_{CN} - 4, Z_{CN} - 2), using two-body kinematics. The method used for determining the spin direction is based on the emission of γ radiation with a particular angular relationship to the spin direction.[8,14] The γ-cascades from rotational nuclei formed in heavy-ion fusion-evaporation reactions have a preponderence of stretched E2 transitions which exhibit a doughnut-like pattern about the spin axis. The spin direction is identified with the short symmetry axis of this pattern. This is close to the compound nucleus spin, i.e. perpendicular to the beam, provided that the misalignement caused by particle emission is small. The γ-pattern for each event was projected on a plane perpendicular to the beam direction and centroid-searching methods were used to determine the angle between the short symmetry axis and the direction of the emitted α-patricle.

In the following analysis, α-particle events corresponding to emission angles near $\theta_{CM} = 90°$ were sorted, imposing different γ-coincidence fold (k_γ gates, or angle with respect to spin (β) gates. Some useful remarks can be made from an inspection of multiplicity decomposed spectra. Fig. 1(a) shows, for ^{114}Sn*, the experimental $\theta_{C.M.} = 90°$ spectra corresponding to k_γ = 11-14 and k_γ = 27-33. The closed circles on the bottom show the total 90° center-of-mass spectrum integrated over k_γ (for $k_\gamma \geq 11$) and β. The corresponding α-particle spectra for ^{170}Yb*, under the same gating conditions, are shown in Fig. 1(b). In both cases, the selected k_γ bins correspond to α-particle emmision from nuclei with an average spin of $\approx 34\ \hbar$ and $\approx 64\ \hbar$, respectively, deduced from statistical model calculations[8,10].

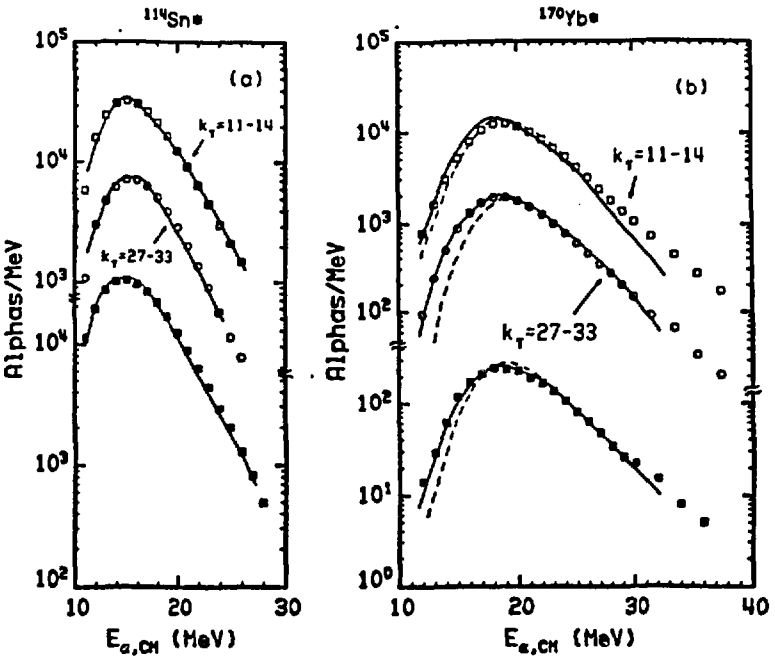

Figure 1. (a) Fold gated 90° center-of-mass alpha-particle spectra from the deexcitation of $^{114}Sn^*$. The open squares correspond to k_γ = 11–14 and the open circles to k_γ = 27–33. The closed squares show the 90° center-of-mass spectrum integrated over k_γ and β. (b) Multiplicity fold gated 90° center-of-mass alpha-particle spectra from $^{170}Yb^*$. The squares correspond to k_γ = 11–14 and the circles to k_γ = 27-33. The closed squares show the 90° center-of-mass spectrum integrated over k_γ and β. The solid and dashed lines are the results of calculations described in the text.

A common trend in both cases is that the k_γ = 11-14 spectra are slightly harder than the k_γ = 27-33 ones. This can be understood in terms of the higher excitation energy selection made by the low k_γ gate. However, the subbarrier trends of the spectra are quite different. For $^{114}Sn^*$, the low k_γ compared to the high k_γ spectrum has an excess of subbarrier alphas, whereas these two regions in the $^{170}Yb^*$ spectra are very similar. The solid lines in Fig. 1(a) are the result of a statistical model calculation with standard parameters.[8,16,17], We We see that there is a good agreement with the data in the whole energy range, for all of the gating conditions. The corresponding calculation for $^{170}Yb^*$ is shown, on Fig. 1(b), by the dashed lines. The k_γ = 11-14 spectrum is underpredicted in the subbarrier region as well as at high energies. In the k_γ = 27-33 bin, the discrepancy is only in the subbarrier region and it has increased. Similarly, the total alpha spectrum is underpredicted at subbarrier energies. In summary, although the behaviour of the alpha particle spectra from $^{114}Sn^*$ is well described by statistical model calculations, we observe a systematic underprediction of the subbarrier parts of the $^{170}Yb^*$ spectra, in a manner which increases with spin.

A striking differece is observed in the trend of the anisotropy coefficients of alpha emission with repect to the spin direction. The anisotropy coefficients A_2 (of a Legendre polynomial expansion) are plotted for the two systems as a function of $E_{\alpha,CM}$ for the indicated k_γ bins in Fig. 2. For $^{114}Sn^*$, we have monotonically decreasing A_2 coefficients (increasing anisotropies) with increasing E_α, in each of the k_γ bins. In contrast with these findings, the A_2 coefficients for $^{170}Yb^*$ have a maximum value (minimum anisotropy) at the evaporation Coulomb barrier ($\approx$ 20 MeV for $^{170}Yb^*$ assumed

spherical) and become more negative (larger anisotropies, with stronger emission perpendicular to the spin direction) at lower and higher E_α values. Compared with the almost linear decrease with E_α observed for $^{114}Sn^*$, we see a deviation in the trend of the experimental correlations below the Coulomb barrier. The $^{170}Yb^*$ data suggest enhanced anisotropies which become larger with decreasing E_α. This enhancement increases with increasing spin.

Both of the data sets are compared with the results of a statistical model calculation with standard parameters in Fig. 2. The pairs of curves are FWHM boundaries of the calculated A_2 coefficients. For $^{114}Sn^*$, we see that the trend of the A_2 coefficients and their absolute magnitude are reproduced by the calculation.

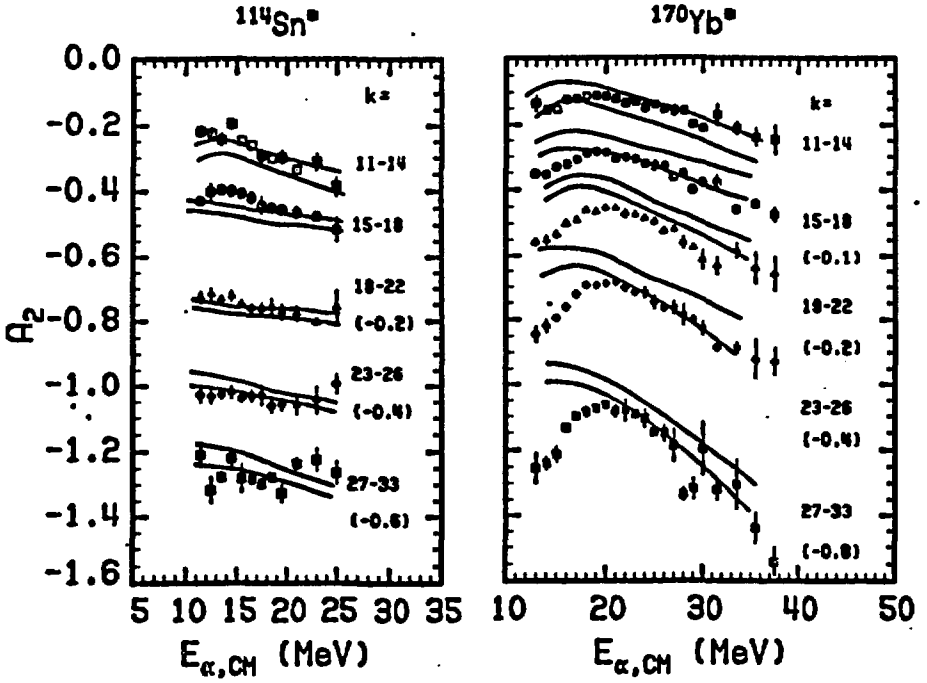

Figure 2. A_2 coefficients as a function of $E_{\alpha,C.M.}$ from the $^{114}Sn^*$ and $^{170}Yb^*$ systems. In both cases, the open squares, circles, closed triangles, diamonds and closed squares correspond to the k_γ bins of 11-14, 15-18, 19-22, 23-26 and 27-33, corresponding to $< I >_\alpha$ for α emission of 34, 43, 51, 59, and 64 $\hbar$, respectively. In some cases the data have been shifted along the A_2-axis by the indicated amount. The pairs of curves are FWHM boundaries of the A_2 coefficients from a statistical model calculation using transmission coefficients from a spherical optical model potential.

The calculated A_2 coefficients, for $^{170}Yb^*$, agree well with the monotonic decrease of the experimental A_2 values above the Coulomb barrier, but do not reproduce the decrease of A_2 at low E_α.

The fact that the observed deviation occurs at emission energies sensitive to barrier penetration effects, has suggested the nuclear deformation as a possible factor for the decrease of the measured A_2 coefficients at low E_α. If the emitting system is deformed with its longest axis perpendicular to the spin direction, the subbarrier α-particles will

be emitted preferentially along this direction (because of the lower Coulomb barrier). This leads to decreasing A_2 coefficients with decreasing E_α. On the other hand, the α-particles above the barrier would not be affected much by the deformation since their emission is mainly determined by the level densities. Therefore, the observed deviation can be interpreted as a deformation effect which increases with spin. The same interpretation accounts also for the discrepancies observed in the multiplicity gated spectra of Fig. 1.

An interesting comparison of the above systems has been made with data from the decay of giant resonances built on excited states of similar compound nuclear systems. Giant resonance data from the decay of ^{166}Er* (61.5 MeV) suggest a two-component resonance in contrast to the decay of ^{108}Sn* (61.2 MeV) where a single resonance peak was observed.

A simulation of deformation effects in the statistical model code was performed in the case of ^{170}Yb*, in order to get an estimate of the effect. For this purpose we employed a variation of the method of equivalent spheres[18], which has been used successfully in the description of subbarrier fusion data with statically deformed targets.

The daughter nucleus was assumed to have a prolate axially symmetric shape described by the deformation parameter β, which was parametrized as $R(\theta) = R_0[1 + X(\beta) + \sqrt{5/4\pi}\beta P_2(cos\theta)]$, where θ is the angle with respect to the symmetry axis and $X(\dot{\beta}) = -\beta^2/4\pi$ is the volume conservation term. Optical model transmission coefficients for protons and alphas were calculated, for all of the nuclei in the cascade, at 9 different angles from 5° to 85° in steps of 10°. At each angle, the optical model radii were scaled according to the above equation. The diffuseness of the of the Woods-Saxon nuclear potential of the spheroid was also modified, so that the normal derivative at each point on an equipotential surface is unaffected by the deformation. The alpha events from the evaporation calculations, emitted at each angle, were sorted and weighted according to the corresponding surface element of the spheroid: $2\pi R^2(\theta)sin\theta\Delta\theta/S$, where S is the nuclear surface: $S = 4\pi R_0^2(1+a_2^2/5)$, $a_2 = \sqrt{5/4\pi}\beta$, including the first order correction term due to deformation.

The result of this calculation for the 90° center-of-mass spectra of ^{170}Yb* is shown in Fig. 1, by the solid lines. A deformation of $\beta = 0.2$ was initially assumed. The result of this calculation for the total alpha spectrum is shown on the bottom of Fig. 1(b) by the solid line and provides a good description of the spin integrated spectrum.

On the same plot, the solid line for the k_γ=11-14 bin ($< I >_\alpha$ =34$\hbar$), shows the calculated spectrum with β=0.2. The subbarrier data points lie between the curves β=0 and β=0.2. In this case, a deformation somewhat smaller than β=0.2 is required to fit the spectrum. On the other hand, for the high spin case k_γ=27-33 ($< I >_\alpha$=64$\hbar$), β=0.2 was insufficient to account for the excess of subbarrier alphas. The solid curve

in the figure, corresponds to β=0.35 and fits closely the spectrum. These calculations demonstrate the extent and the angular momentum dependence of the effect. The originally deduced β=0.2 was based on the total 90° center-of-mass spectrum and represents an average over different deformed shapes.

The calculated A_2 coefficients, using the above logic, show a trend approaching the experimental data at subbarrier energies. However, no quantitative statement was made from such comparisons, because our present formalism for the calculation of the angular correlations is limited to spherically symmetric emitters. More refined calculations are required for this purpose.

Summarizing, the distinct differences in the alpha decay properties of the compound nuclei ^{114}Sn and ^{170}Yb have been interpreted in terms of deformation effects. For ^{170}Yb*, our calculations have demonstrated the angular momentum dependence of the effect in the 90° center-of-mass spectra, besides the one observed in the trend of the anisotropy coefficients of alpha emission with respect to the spin direction. One should keep in mind that the α-particle emission probe for studying nuclear shapes at high E* involves a broad range of initial excitation energies which contribute in low energy particle emission.[10]

3. STRUCTURE EFFECTS AND PROTON EVAPORATION SPECTRA

Compound nuclei that decay to residual nuclei with large deformations, such as superdeformed nuclei with discrete level structures, may be expected to have themselves significant deformations which persist to sufficiently high excitations of the order of at least one nucleon binding energy above the yrast line. In this case particle emission can be significantly influenced by nuclear shape effects. Furthermore, it is quite possible that structure effects can be observed on the shape of the charged particle evaporation spectra particularly near and below the emission barrier. The experimental observation of the existence of such effects is important both on its own merit and for providing important information about methods of populating the so called "hyperdeformed" structures in nuclei.

We report here on the results of an attempt to investigate the connection between proton emission from a decaying compound nucleus and underlying structural features in the final product. In this work we have selected for study ^{82}Sr as the final nucleus, because it has been predicted to be a good candidate for superdeformation.[19]

The experiment was performed at the Oak Ridge Heavy Ion Research Facility. The ^{82}Sr nuclei were produced by the ^{52}Cr(^{34}S, 2p2n)^{82}Sr reaction by bombarding a stack of self-supporting ^{52}Cr target foils with a 130 MeV ^{34}S beam. The experimental setup consisted of the ORNL Compton suppression spectrometer with 18 Ge detectors, which recorded the discrete γ-ray spectra from the reaction. The associated total γ-ray

multiplicity and total energy were recorded with the Spin Spectrometer. The protons and α particles were detected with the 4π CsI(Tl) Dwarf Ball .[15] This system provided both high resolution γ-ray spectroscopic information and definite exit channel selection. The 72-element Dwarf Ball also provided light charged particle spectra and angular correlation information. The apparatus was triggered by two or more Ge detectors firindg in coincidence with any element of the Dwarf Ball. A total of 1.6×10^8 such events were collected and processed.

Figure 3 shows a scatter plot of the slow vs. tail map from a 42° CsI(Tl) detector. The γ-rays, protons and α particles are well separated. This was achieved by placing two time gates 400 ns (slow) and 1500 ns (tail) wide starting at times 0 and 1500 ns from the front of each pulse, respectively, and integrating the corresponding charge.

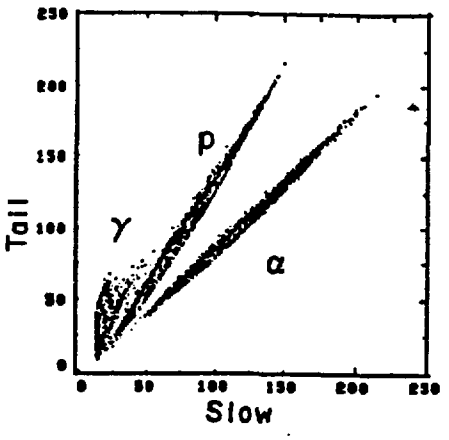

Figure 3. Scatter plot of the slow vs. tail light output of a CsI(Tl) detector in the Dwarf Ball showing the α, proton and γ-ray identification.

The particle identification in the Dwarf Ball utilizes the different time characteristics of the scintillation output of the CsI(Tl) (pulse shape discrimination). Excellent separation for all energies was achieved between proton and α pulses from each other and from γ-rays or neutrons for the detectors forward of 102° in the laboratory ($\sim$ 120° center-of-mass). The protons with subbarrier energies could be clearly identified for yields $\sim$ 1/20 of that at the most probable value. The proton spectra sorted in this way contained $\sim$ 65% of the total proton yield. At larger angles due to kinematic forward focussing some of the subbarrier protons cannot be distinguished from α particles and therefore the detectors at these angles were used for channel selection, but not for particle spectra. The measured overall detection efficiency for proton detection was 85% of 4π (4 detectors out of 72 were removed for the beam, target rod and viewer port, and one detector did not operate). This caused $\sim$ 28% of the events with two protons to be identified as involving only one proton. The Ge energy spectra coincident with 2 protons involved primarily ^{82}Sr γ-rays with no contamination from the 1pxn or the αxn emitting channels. During the experiment, the most forward detectors were operated at a rate of $\sim$ 7000 c/s. A close examination of proton and α particle spectra recorded

on different tapes revealed gain shifts up to 8% in the tail component, while the slow component was considerably more stable. Thus, gain shift corrections for every 2×10^6 events were applied for the tail component. This ensured good particle identification for the complete data set. The more stable slow component was calibrated for energy measurements using the $^{12}C(p,p')$ reaction at 9.0 and 20.0 MeV. The energy calibration uncertainties were estimated to be less than 3% for all but the 24° detectors for which uncertainty may be as large as 6%.

The particle energies were converted event by event to the center of mass system. The centroid angles for each detector in the laboratory system were used in deriving the center-of-mass energy and angle, assuming compound nucleus formation and decay to one proton. Proton energy spectra were sorted using the detectors forward of 102°, when 2 protons were identified in the complete Dwarf Ball and for three k_γ gates of 3-9, 10-14, and 15-25. Further selection was made by placing gates on discrete γ-rays associated with various rotational bands. The background to the proton spectra associated with the underlying Compton contribution in the Ge peaks were subtracted by placing equal width gates near each γ peak. Care was exercised to avoid peaks that are known to be doublets. Thus, for the four main bands, gates placed on single γ-ray peaks for transitions up to spin 10 gave spectra of good statistical quality. For higher spins, the proton spectra for two or three transitions were added to provide spectra of improved statistical quality, but in each case the spectra for each gate were examined for consistency.

Angular correlations of the coincident protons were recorded at 24°, 42°, 50°, 63°, 68°, and 78° in the laboratory, corresponding to angles ranging from ~ 30° to 95° in the center of mass.

The level scheme for ^{82}Sr was constructed from a γ-γ matrix obtained by requiring that at least one proton was detected and that the γ-ray multiplicity exceeded 10. The matrix thus constructed was dominated by γ-rays from ^{82}Sr. Figure 4 shows a partial level scheme for ^{82}Sr constructed from these data. Two new bands were established and four previously known bands were extended from 20 to 27 $\hbar$. The even parity band 4 is yrast for spins between 10 and 22 $\hbar$. The odd spin band 2 becomes yrast at very high rotational frequencies ($I \geq 23$).

Proton spectra coincident with the $2^+ \rightarrow 0^+$ ground transition are shown in Fig. 5 for the three k_γ gates. For purposes of comparison, the spectra are shown normalized to the same total counts. The spectra at the most probable value have 1.1×10^4, 3.5×10^4, and 2.0×10^4 counts per 0.5 MeV interval. As one moves to the high k_γ gates, the spectra are seen to shift to lower energies, with a lower apparent emission barrier, but the slopes at high energies are similar. This is understood in terms of the decreasing available thermal excitation due to increased spin range in the entry

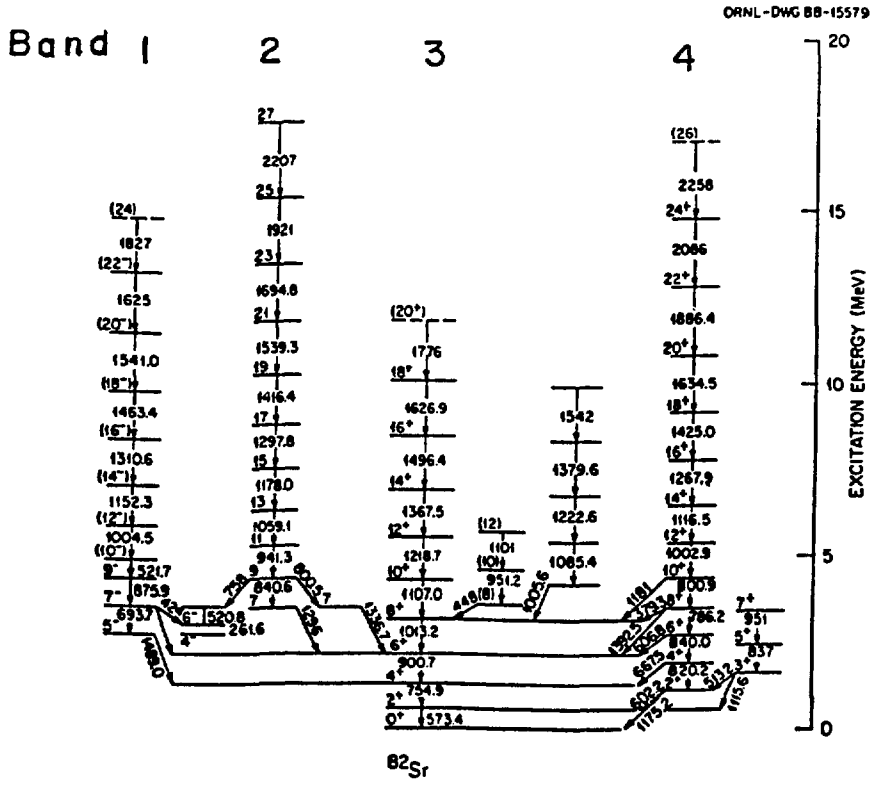

Figure 4. Partial level scheme for ^{82}Sr.

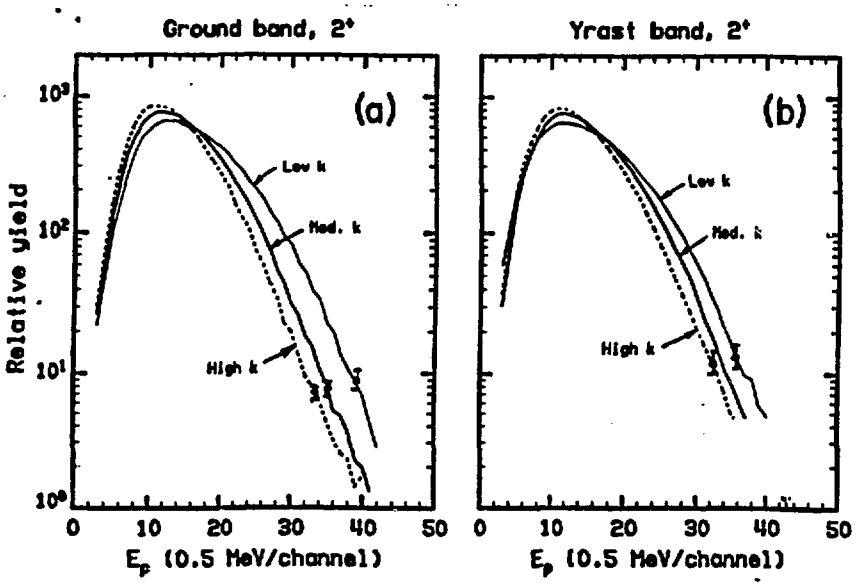

Figure 5. Panel (a) shows the proton spectra coincident with the $2^+ \rightarrow 0^+$ transition in the ground band (band 3) for the three k_γ gates. The spectra are normalized to the same total counts for comparison. It is seen that the proton emission barrier decreases as k_γ increases. Panel (b) shows the proton spectra coincident with the 2^+ level in band 4 (see Fig.4) for the three k_γ gates. Here the proton emission barrier is essentially independent of the k_γ gating, although the high energy yield decreases as k_γ increases.

region ($I \sim$ 4-19, 17-29, and 26-45 $\hbar$, at mean yrast energies of ~7, 14 and 23 MeV, respectively). In contract to this, the proton spectra associated with the 2^+ level of

band 4 (non-yrast at this spin, but yrast at spins 12 to 22$\hbar$) show similar emission barriers for the three k_γ gates (Fig. 5b). As the k_γ is decreased, the spectra shift somewhat to higher energies, but the slope parameters at high E are similar. The differences between the spectra coincident with the different 2^+ states suggest that some structural effects and/or feeding patterns may be responsible.

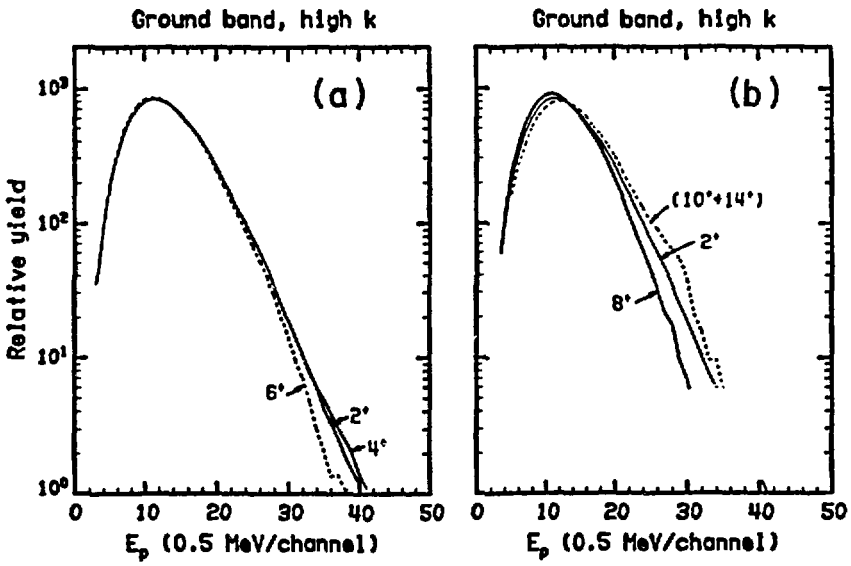

Figure 6. Panel (a) shows proton spectra coincident with γ-rays from the $2^+, 4^+$, and 6^+ levels in the ground band 3 for the high k_γ gate. The spectra are normalized to the same total counts for ease of comparison. The spectra are remarkably similar. Panel (b) shows proton spectra coincident with the 8^+ and the sum of $(10^+ + 14^+)$ levels in the same ground band 3 and for the high k_γ gate. The 2^+ spectrum is also shown for comparison. Significant differences are seen *(see text)*.

In order to explore this possibility, we compare in Fig. 6(a) the proton spectra coincident with the γ-rays from the 2^+, 4^+, and 6^+ states in the ground band 3 and for the high k_γ gate. Clearly, the spectra are very similar, with a hint of softening of the spectra for the 6^+ state. We note that the 2^+ and 4^+ and for the most part the 6^+ levels receive practically all the feeding from all the bands in ^{82}Sr, whereas the 8^+ level is only fed from higher spin members of the ground band and to a significant fraction by the yrast band 4. Levels above the 8^+, however, are only populated by the decay of the levels of the continuation of the ground band. The proton spectra coincident with the 8^+ and the sum of 10^+ and 14^+ levels are compared in Fig. 6(b) with the 2^+ spectrum. It is seen that the spectra for the 8^+ and $10^+ + 14^+$ levels shift toward lower and higher emission barriers, respectively. This unexpected behaviour is explained below by considering spectra associated with high spin states in the four major bands in ^{82}Sr.

Next we note that the proton spectra from individual levels within each band having spins higher than 10$\hbar$ were found to be similar to each other, but differ considerably.

for different bands. This is shown in Figs. 7(a) and (b) for protons associated with the levels indicated. There are three striking features in these spectra: (1) for the same k_γ gate the emission barrier shifts by as much as 1 MeV toward lower values in going from the ground band to the yrast band; (2) the higher energy region also shows differences with the ground band having excess high energy protons; and (3) for the high and medium k_γ gates only the higher energy part of the spectrum changes, while the spectral shapes at and below the barrier are the same for each band. The latter is to be contrasted with the 2^+ spectra of Fig. 5(a) where both the low and high energy portions of the spectra show differences as k_γ is increased. The above features are at first surprising, since in the standard statistical evaporation picture one should expect no differentiation between bands, because the entry state population is at spins greater than $\sim 17\hbar$ and $26\hbar$ for the medium and high k_γ gates, respectively, which are well above the gating discrete transitions.

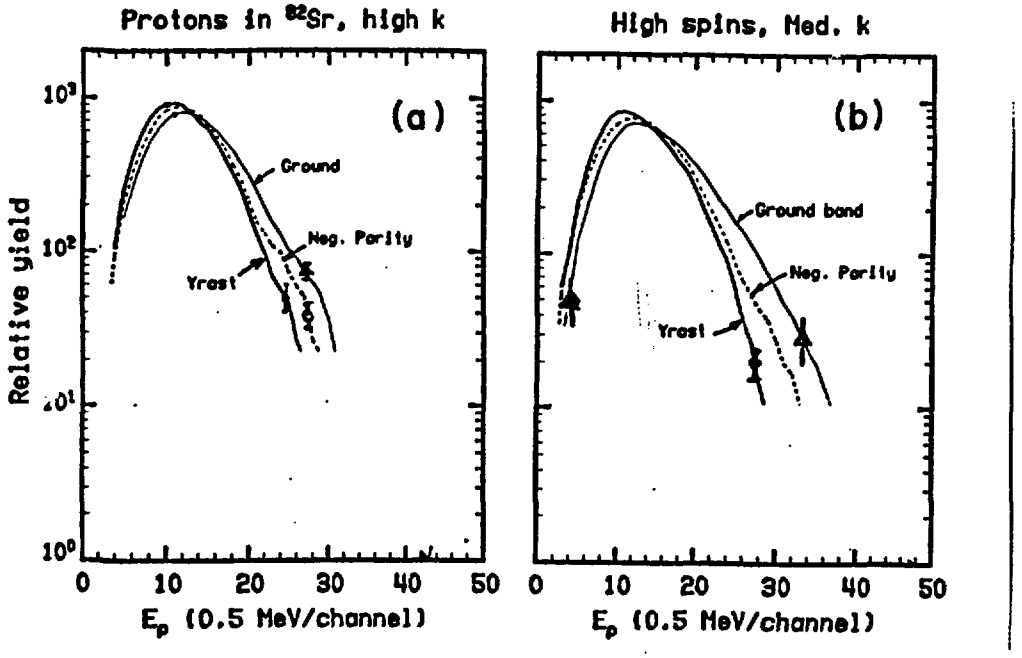

Figure 7. Panel (a) shows proton spectra from the high k_γ gate coincident with transitions from the $(10^+ + 14^+)$ levels of the ground band 3 (thin line), from the $(14^- + 16^-)$ levels of the negative parity band 1 (dashed line), and from the $(14^+ + 16^+)$ levels in the yrast band 4 (thick line). Shifts as large as 1 MeV are seen in going from the ground to the yrast band gates. Panel (b) shows proton spectra from the medium k_γ gate. The curve labels are for the same as in (a).

DISCLAIMER

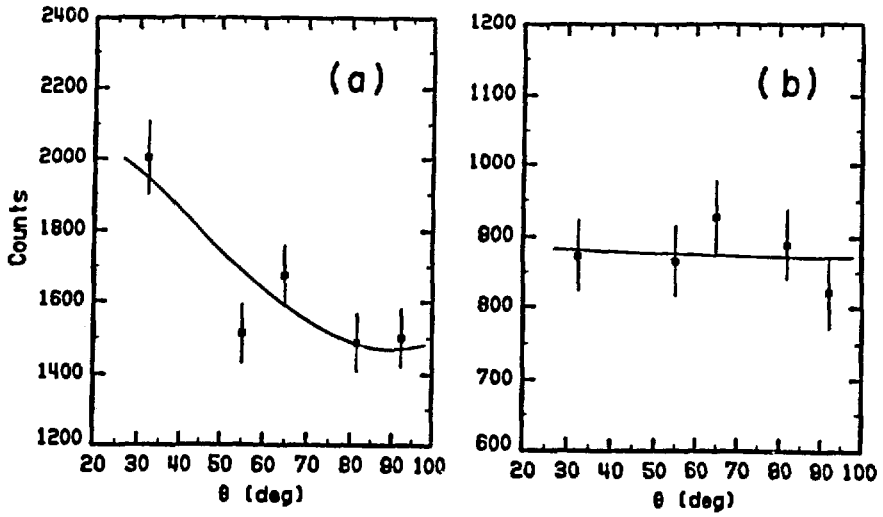

Figure 8. Angular correlations in the center-of-mass of the protons in the energy range 4.0-5.0 MeV for the high k_γ gate coincident with the $(14^+ + 16^+)$ tranistions of the yrast band 4 (left panel), and the $(10^+ + 14^+)$ transitions of the ground band 3 (right panel).

A careful examination of the measured k_γ distribution coupled with energy balance considerations require that the entry line for this channel be only a few MeV above the yrast line. This suggests that a sizeable fraction of the population of the yrast band may occur by direct proton emission at or close to the yrast line. This mechanism would explain items (1) and (3) mentioned above. The observation in point (2) can be understood in terms of differences in thermal energy across the k_γ gate, provided one can argue that the ground band at high spin is preferentially populated by the connecting "statistical" γ-rays only from the higher I and E* region in the k_γ gate. This mechanism cannot, however, account for point (3) above, namely the independence of the subbarrier shape or k_γ gate.

If this picture with significant direct population of the yrast line by stretched proton emission is correct, then we would expect the subbarrier region to show a substantial enhancement of the proton angular correlations with respect to the beam direction.[20] This is indeed supported by the angular correlations. The angular correlations were constructed by selecting 5 proton energy gates, which give comparable counts. As an example, the correlation for high k_γ and the 4.0-5.5 MeV proton bin are shown in Fig. 8 for the yrast and ground band $(14^+ + 16^+)$ and $(10^+ + 14^+)$ gates, respectively. The correlations were fitted by least square procedure to the expression $A_0[1 + A_2 P_2(\cos\theta)]$, where $P_2(\cos\theta)$ is the Legendre polynomial. Then the $W(0°)/W(90°)$ anisotropies were calculated from the fit and these were then divided by the proton anisotropy associated with the $2^+ \rightarrow 0^+$ ground transition. This procedure reduces considerably any systematic errors due to uncertainties in the proton energy calibrations. The resulting anisotropy ratios for the yrast band $(14^+ + 16^+)$ and the ground band $(10^+ + 14^+)$ are shown in Fig. 9(b). The horizontal bars give the range of the proton energy gates.

In Fig. 9(a) the A_0 coefficient expressed as counts/MeV are shown for comparison. Thus, a significant enhancement of the yrast band anisotropy at and below the barrier is clearly seen relative to that of the ground band. This substantiates the above interpretation.

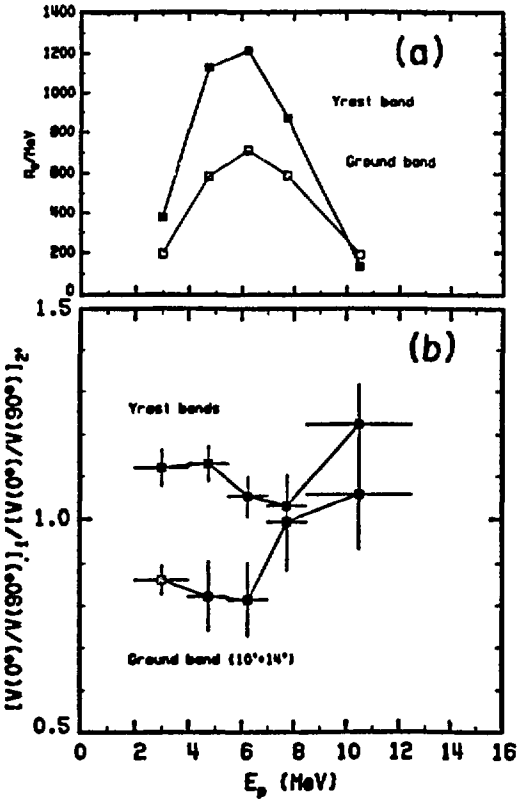

Figure 9. The lower panel shows the anisotropy ratios for the protons from high k_γ gate coincident with the high spin transitions (Fig. 8) in the yrast band 4 (full squares) and the ground band 3 (open squares), relative to that for the $2^+ \rightarrow 0^+$ transition to the ground state. The horizontal error bar give the widths of the proton energy gates used. Thes were chosen to give comparable statistics in the correlations. The upper panel shows the corresponding portions of the proton energy spectra used in the energy gates for the angular correlations. The quantity plotted are the A_0 coefficients per MeV obtained from the angular correlation fits.

The angular correlations for the middle k_γ gate show a similar, but somewhat reduced enhancement, but the anisotropy for the ground band is not reduced significantly over that for the $2^+ \rightarrow 0^+$ ground transition.

This can come about from the instability of nuclei near the yrast region with large spins toward emission of nucleons. Such instabilities could be connected to the occupation of $h_{11/2}$ resonance states in the nucleus.[20] These effects may in turn be related to the competing decay modes by nuclear emission from superdeformed nuclei.

REFERENCES

1. P.J. Twin, B.M. Nyako, A.H.Nelson, J. Simpson, M.A. Bentley, H.W. Cranmer-Gordon, P.D. Forsyth, D. Howe, A.R. Mokhtar, J.D. Morrison, J.F. Sharpey-Schafer and G. Sletten, Phys. Rev. Lett. **57** (1986) 811.
2. J. Dudek, T. Werner and L.L. Riedinger, Phys. Lett. **B211**, 252 (1988).
3. S. Cohen, F. Plasil, and W. Swiatecki, Ann. of Physics, N.Y., **82**, 557 (1974).
4. L.A. Goodman, Phys. Rev. **C37**, 2162 (1988).
5. K.A. Snover, Ann. Rev. Nucl. Part. Sci., **36**, 545 (1986).

6. M.Blann and T.T.Komoto, Phys. Scr. 24, 93 (1981).
7. J.M. Alexander, D.Guerreau and L.C. Vaz, Z. Phys. A **305**, 313 (1982).
8. F.A. Dilmanian, D.G. Sarantites, M. Jääskeläinen, H. Puchta, R. Woodward, J.R. Beene, D.C. Hensley, M.L. Halbert, R. Novotny, L. Adler, R.K. Choudhury, M.N. Namboodiri, R.P. Schmitt, and J.B. Natowitz, Phys. Rev. Lett. **49**, 1909 (1982).
9. Z. Majka, D.G. Sarantites, L.G. Sobotka, K.J. Honkanen, E.L. Dines, L.A. Adler, Ze Li, M.L. Halbert, J.R. Beene, D.C. Hensley, R.P. Schmitt and G. Nebbia, Phys. Rev. Lett. **59**, 322 (1987).
10. N.G. Nicolis, D.G. Sarantites, L.A. Adler, F.A. Dilmanian, K.J. Honkanen, Z. Majka, L.G. Sobotka, Z. Li, T.M. Semkow, J.R. Beene, M.L. Halbert, D.C. Hensley, J.B. Natowitz, R.P. Schmitt, D. Fabris, G. Nebbia and G. Mouchaty, *'The Variety of Nuclear Shapes'*, edited by J.D. Garrett, C.A. Kalfas, G. Anagnostatos, R. Vlastou, (World Scientific, 1987) pp. 526–536. (the complete study has been submitted for publication in Phys. Rev. C).
11. Z. Majka, M.E. Brandan, D. Fabris, K. Hagel, A. Menchaca-Rocha, J.B. Natowitz, G. Nebbia, G. Prete, B. Sterling and G. Viesti, Phys. Rev. C **35**, 2125 (1987).
12. L.C. Vaz and J.M. Alexander, Z. Phys. A **318**, 231 (1984).
13. M. Jääskeläinen, D.G. Sarantites, R. Woodward, F. A. Dilmanian, J.T. Hood, R. Jääskeläinen, D.C. Hensley, M.L. Halbert, and J.H. Barker, Nucl. Instr. Meth., **204**, 385 (1983).
14. K.J. Honkanen, F.A. Dilmanian, D.G.Sarantites, and S.P. Sorensen, Nucl. Instr. Meth. **257**, 233 (1987).
15. A CsI(Tl) version of the Dwarf Ball system described in: D.G. Sarantites, L.G. Sobotka, T.M. Semkow, V. Abenante, J. Elson, J.T. Hood, Z. Li, N.G. Nicolis, D.W. Stracener, J. Valdes and D.C. Hensley. Nucl. Instr. Meth. **A264**, 319 (1987).
16. A. Gavron, Phys. Rev. C **21**, 230 (1980); modification PACE2S by J.R. Beene.
17. N.G. Nicolis and D.G. Sarantites, submitted in Phys. Rev. C.
18. R.G. Stokstad and E.E. Gross, Phys. Rev. C **23**, 281 (1981).
19. W. Nazarewicz *et al.*, Nucl. Phys. **A435**, 397 (1987).
20. T. Dossing, S. Frauendorf, and H. Schulz, Nucl. Phys. **A287**, 137 (1977).